

Morphological analysis of olivine grains annealed in an iron-nickel matrix: Experimental constraints on the origin of pallasites and on the thermal history of their parent bodies

Kazuto SAIKI,^{1*} Didier LAPORTE,² Daniel VIELZEUF,² Satoru NAKASHIMA,³ and Pierre BOIVIN²

¹Research Institute of Materials and Resources, Faculty of Engineering and Resource Science, Akita University,
1–1 Tegata Gakuen-Machi, Akita 010–8502, Japan

²Laboratoire Magmas et Volcans, CNRS et Université Blaise Pascal, Observatoire de Physique du Globe,
5 Rue Kessler, F-63038, Clermont-Ferrand Cedex, France

³Department of Earth and Planetary Sciences, Tokyo Institute of Technology, 2–12–1 Ookayama, Meguro-ku, Tokyo 152–8551, Japan

*Corresponding author. E-mail: ksaiki@rimr.akita-u.ac.jp

(Received 15 November 2001; revision accepted 17 March 2003)

Abstract—Two types of pallasites can be distinguished on the basis of the grain shape of olivine (rounded or angular). It has been suggested that these two types of textures resulted from different degrees of annealing at high temperature in the parent body. In order to characterize the kinetics of rounding of olivine grains in an Fe-Ni matrix, we carried out a series of annealing experiments using a mixture of olivine and Fe-Ni powder. We were able to reproduce, at a miniature scale, the range of textures in pallasites. The rate of rounding was rapid enough to be observed and measured at the scale of a few micrometers to 20 μm , even though the experiments were performed below the solidus of the Fe-Ni metal. For instance, grains $\approx 14 \mu\text{m}$ in diameter became nearly spherical within 7 days at 1400°C. For the morphological analysis of olivine grains, we used two independent techniques: the “critical diameter method” and the “Gaussian diffusion-resample method,” a new technique specially developed for our study. Both techniques indicate that the rounding time scale is proportional to the cube of the grain size and that morphological adjustments in our experiments occurred by volume diffusion in the olivine lattice, not by surface diffusion along the olivine-metal boundaries.

We used our experimental data to estimate the time scales required for the development of olivine-metal textures in natural pallasites. We determined that small scale rounding of olivine grains in a solid metal matrix can be produced within relatively short time intervals: ≈ 100 years to produce rounded olivine grains 0.1 mm in radius at 1300–1400°C.

INTRODUCTION

Pallasites are stony-iron meteorites mainly composed of closely packed grains of olivine embedded in a nickel-iron matrix. Metal and olivine are in approximately equal weight percentages and coexist with minor phases such as troilite (FeS) and schreibersite (Fe₃P; Buseck 1977). According to a comparative study of trace and minor elements concentrations in Fe metal (Scott 1977a), pallasites are separated into two groups: main group and Eagle Station group. These two groups have been considered as originating from different parent bodies. Boesenberg et al. (1995) reported a third group of pallasites from the evidence of oxygen isotope data: the pyroxene pallasites with 86 vol% metal, rounded to subrounded olivine, and orthopyroxene, chromite, and merrillite.

Two textural kinds of pallasites may be distinguished depending on the shape of olivine grains (Buseck 1977, Scott 1977b). Many pallasites, such as Brenham (Fig. 1a) or Thiel Mountains, contain rounded olivine grains. In other pallasites, such as Eagle Station (Fig. 1b), olivines display macroscopically sharp edges and range from polyhedral grains to small angular fragments. At a smaller scale of observation, the olivine grain edges in these pallasites are rounded, and it has been suggested that the rounding of grain edges was the result of annealing of olivine fragments in a metallic matrix at high temperature.

The origin of pallasites is still controversial. Pallasites are generally considered to come from the core-mantle boundary of differentiated parent bodies, but neither the processes by which metal and olivine are intimately mixed nor the thermal history and the size of the parent bodies are

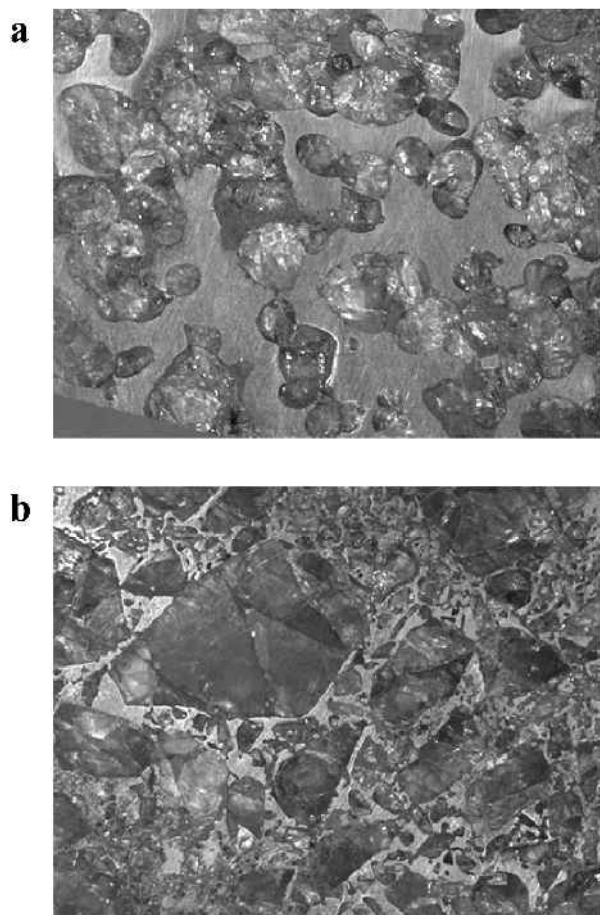


Fig. 1. Photographs of: a) Brenham pallasite (with rounded olivines), and b) Eagle Station pallasite (with angular olivines). The width of both photographs is 5 cm. These samples are owned by the Center for Meteorite Studies, Arizona State University, Tempe.

well understood. The association of olivine and metal in pallasites has been interpreted either as a primary feature (Buseck 1977; Wood 1978; Takahashi 1983; Greenberg and Chapman 1984) or as a secondary feature (Scott 1977b; Ulff-Møller et al. 1998; Wasson et al. 1999).

Pallasites as Igneous Cumulates

In this model, the olivine-metal mixture is a primary feature, which results from the internal differentiation of a small parent body (50–100 km in diameter according to Greenberg and Chapman 1984). In a simple version of this model (Wood 1978; Greenberg and Chapman 1984), the first stage was the complete melting of the parent body and the formation of a metallic core. Then, olivine began to crystallize in the molten silicate mantle, settled down, and formed cumulates of closely packed grains. The lower part of the cumulate was forced into the core by the weight of the overlying olivine: over about 10% of the total height of the

cumulate. The interstices between the olivine grains were filled with liquid iron, giving rise to a pallasite-like texture. Takahashi (1983) proposed a slightly different version of the cumulative model in which the olivine-metal mixture in pallasites result from an incomplete separation of molten metal from silicates at depth in a partially molten parent body.

Catastrophic Mixing of Olivine and Metal

According to Scott (1977b), melting and differentiation of a chondritic parent body first resulted in the complete separation of a metallic core and a silicate mantle with a pure olivine layer at the bottom. Three processes were then involved in the development of the olivine-metal textures in pallasites: 1) fragmentation of the dunitic deeper mantle; 2) intrusion of the underlying molten metal into the brecciated dunite; and 3) high-temperature annealing of the olivine-metal mixture to produce the range of textures observed in pallasites. Steps 1 and 2 were presumably contemporaneous and could have resulted, for instance, from a catastrophic impact. In Scott's (1977b) model, the range of olivine-metal textures corresponds to different degrees of annealing: if the olivine-metal mixture is rapidly cooled, the olivine grains in the final texture are macroscopically angular and only show a small-scale rounding of their grain edges. On the contrary, pallasites with large rounded olivine grains and near-equilibrium olivine-metal textures result from a slow cooling and a long annealing stage.

The size of the pallasite parent bodies and their thermal history are still matters of debate. Buseck and Goldstein (1969) analysed Fe-Ni diffusion profiles in Widmanstätten structures in pallasitic metal and deduced cooling rates of $\approx 1^\circ\text{C}$ per million years from 700°C to 300°C . However, Narayan and Goldstein (1983) and Yang, Williams, and Goldstein (1997) concluded that these values were underestimated. According to Yang, Williams, and Goldstein (1997), pallasite cooling rates would lie in the range $2\text{--}5^\circ\text{C}$ per million years. The very low cooling rates deduced by Buseck and Goldstein (1969) were the strongest evidence for formation of pallasites deep in parent bodies many hundreds of kilometers in diameter. With the revised cooling rates, the diameter of the pallasite parent bodies could be much smaller: down to 50 km (Greenberg and Chapman 1984). Miyamoto and Takeda (1993, 1996) and Miyamoto (1997) attempted to constrain the thermal history of pallasites by measuring FeO, MgO, CaO, etc. concentration profiles in olivine grains. The modelling of concentration profiles is equivocal, however, and depends strongly on the temperatures at which the chemical zoning is assumed to develop. The cooling rates computed by Miyamoto (1997) range from $20\text{--}200^\circ\text{C}$ per year for linear cooling from 1100°C to 600°C to $\approx 100^\circ\text{C}$ per million years for linear cooling from an initial temperature of 600°C . Cooling rates of $20\text{--}200^\circ\text{C}$ per year correspond to burial depths of several tens of meters under a solid rock;

cooling rates of 100°C per million years are in good agreement with revised metallographic cooling rates and correspond to burial depths of a few tens of kilometers. Additional arguments against formation of pallasites at depths of a few hundred kilometers were provided by recent studies of short-lived chronometers and Re-Os systematics (e.g., Shen, Papanastassiou, and Wasserburg 1998; Lugmair and Shukolyukov 1998). These studies yielded a time scale of 20 Ma for partial melting, differentiation, and solidification of pallasite parent bodies. Assuming that pallasites formed at the core-mantle boundary, this short time scale implies that the diameter of the parent body was ≤ 20 km: larger parent bodies (for instance, ≈ 60 –100 km in diameter) would indeed have preserved partially molten metal over ~ 100 Ma (Shen, Papanastassiou, and Wasserburg 1998). Alternatively, if pallasites formed closer to the surface, they could originate from parent bodies larger than 20 km in diameter.

The olivine-metal textures, especially the grain shape of olivine, are very important features that can be used to constrain the origin of pallasites. Toriumi (1979, 1981) developed a theoretical model of the rounding of a small mineral inclusion isolated in a solid matrix. He estimated the rounding kinetics of quartz inclusions in albite and of mineral inclusions in upper mantle peridotite. Ohtani (1983) applied Toriumi's kinetic theory to olivine in pallasites and showed that the shape of olivine grains may be used to determine the thermal history of the pallasite parent body. So far, however, there is no accurate experimental data to predict the kinetics of olivine rounding in metal. We conducted a series of annealing experiments of olivine-metal mixtures in which we were able to reproduce at a miniature scale the main textural features of pallasites. Our main experimental results and their implications for the kinetics of olivine rounding and for the thermal history of pallasite parent bodies are presented in this paper.

EXPERIMENTAL TECHNIQUES AND RUN PRODUCT ANALYSIS

Overview

In order to characterize the rounding kinetics of olivine in an iron-nickel matrix, we performed a series of piston-cylinder experiments in which a mixture of San Carlos olivine, iron, and nickel was annealed at $P = 1$ GPa and T in the range of 1200 to 1450°C. Three sets of experiments of increasing durations (4 hr, 27 hr, and 7 d) were conducted at 1200, 1300, and 1400°C. These sets were complemented by three 7-day experiments at 1250, 1350, and 1450°C to characterize more properly the effect of temperature on kinetics. A summary of run information is given in Table 1.

Starting Materials

San Carlos olivine (9 mole% fayalite; Table 2) was

selected because of its similarity in chemical composition to the olivine in the main group pallasites (10.5–13 mole% fayalite; Scott 1977b). The olivine was ground to a fine powder and sieved with a 20 μm mesh. A metal fraction with a Ni content of 10 wt% was prepared by mixing reagent-grade Fe and Ni powders. This nickel content was chosen to reproduce the metal composition of the main group pallasites (7.8 to 11.7 wt% Ni; Scott 1977a). A homogeneous mixture of olivine and metal was obtained by mixing and mild grinding in an agate mortar. The weight percentage of San Carlos olivine in the mixture is 7.8%, corresponding to a volume percentage of 16.7%. This figure is low compared to the average olivine vol% in pallasites (65%; Buseck 1977) and was aimed at minimizing olivine grain-to-grain contacts during annealing.

Apparatus

The experiments were performed in a 3/4-inch piston cylinder apparatus in the Laboratoire Magmas et Volcans, Clermont-Ferrand. The sample crucibles were 7.8 mm long cylinders of polycrystalline MgO with a 4 mm long and 3.5 mm inner diameter chamber. The chemical composition of polycrystalline MgO in wt% is: MgO, 99.5; CaO, 0.2; SiO₂, 0.1; Al₂O₃, 0.1; Fe₂O₃, 0.1 (plus C at 100 ppm level, and B and S at 10 ppm level). The sample chamber was packed with ≈ 140 mg of olivine-metal mixture, and then covered with a 1.4 mm thick MgO lid that separated the sample from the thermocouple tip. The 3/4-inch assemblies consisted of an outer NaCl sleeve enclosing a pyrex glass sleeve in which the graphite furnace was fitted. Crushable MgO and pyrex inserts were used to position the sample chamber in the hot spot of the assembly. Due to pressurization and compaction, the height of the sample chamber and the thickness of the MgO lid were reduced to 2.8 mm and 1 mm, respectively, at the end of an experiment. The hot-piston-in technique was used for all the piston-cylinder experiments (see Laporte (1994) for a detailed description of the pressurization and heating procedures). No friction correction was applied (run pressure is estimated to be accurate to ± 50 MPa). Temperature was controlled with W₉₅Re₅/W₇₄Re₂₆ thermocouples. Power output was monitored to ensure that no long term temperature drift occurred during a run. The experiments lasted from 4 hr to 7 d and were terminated by shutting off the power to the apparatus. The initial quench rate was 60–70°C per second.

Analytical Methods

At the end of an experiment, the sample was cut lengthwise in two, mounted in epoxy, and polished with 1.0 and 0.3 μm alumina grit. Textures of polished samples were characterized by reflected light microscopy and scanning electron microscopy (SEM) using secondary electron imaging and, to a lesser extent, backscattered electron imaging. For quantitative

Table 1. Summary of experiment.

Sample number	Temperature (°C)	Duration ^a	Eroded area EA^{*b}	Critical diameter D_C (μm)
1	1400	4 h	0.271	4.5
2	1400	27 h	0.234	6.5
3	1400	7 d	0.134	13.9
6	1200	7 d	0.244	4.3
7	1200	4 h	0.288	1.6
8	1200	27 h	0.247	3.2
10	1300	7 d	0.160	8.7
12	1250	7 d	0.200	n.d. ^c
13	1350	7 d	0.144	11.7
14	1450	7 d	0.120	17.1
16	1300	27 h	0.255	3.7
17	1300	4 h	0.283	2.8

^ah = hours; d = days.

^b EA^* is the eroded area computed for a filter aperture of 3.5 pixels. The detailed definition of morphological parameters EA^* and critical diameter is described in the Morphological Analysis section.

^cn.d. = not determined.

Table 2. Average compositions (wt%) of San Carlos olivine and representative compositions of olivine in the experimental products.

	San Carlos	1200°C (4 hr)		1400°C (7d)	
	(n = 4)	core	rim	core	rim
SiO ₂	41.7	40.58	40.03	41.06	40.66
CaO	0.04	0.09	0.08	0.03	0.01
Cr ₂ O ₃	0.04	0.08	0.08	0.00	0.02
MnO	0.13	0.09	0.00	0.08	0.11
FeO	8.76	9.50	9.25	9.73	9.80
NiO	0.27	0.31	0.38	0.11	0.12
Al ₂ O ₃	0.02	0.07	0.00	0.09	0.06
MgO	49.61	48.43	48.59	49.86	49.45
Total	100.6	99.15	98.41	100.96	100.23
Mg'	0.910	0.901	0.904	0.901	0.900

analysis of grain shape, the SEM images were stored as grey level images of 768 by 576 pixels that were subsequently processed using the software Scion Image version β3 for Windows (a free PC version of NIH Image, available from Scion Corporation [<http://www.scioncorp.com>]; NIH Image is a public domain image processing and analysis program for Macintosh, developed at the Research Services Branch of the National Institute of Mental Health, a part of the National Institute of Health, USA [<http://rsb.info.nih.gov/nih-image/>]).

A three-dimensional (3D) insight into the shape of olivine grains was obtained by immersing the polished samples in Nital for 20 min to 1 hr to dissolve the metallic matrix (Nital is a 2:100 volume mixture of nitric acid and ethanol). We checked that Nital dissolved only the metal and did not damage the olivine grains at least for etching durations of 1 hr or less.

Compositions of starting materials and run products were determined with a Cameca-Camebax electron microprobe; analytical conditions were 15 kV, 11 nA, and counting times of 10 s.

RESULTS

Overall Textures, Parageneses, and Phase Compositions

Overall Textures

The main textural features of our experimental products are shown in the secondary electron SEM images of Figs. 2 and 3. For all the experiments at $T \leq 1400^\circ\text{C}$, the textures are characterized by a population of dark olivine grains embedded in a bright FeNi matrix (the polycrystalline texture of the matrix was revealed by nital etching, as discussed below). All samples, even the long-duration ones, exhibit a wide dispersion of olivine grain sizes: from less than 1 μm to a few tens of μm.

The rounding of olivine grains with increasing run duration is best illustrated in the kinetic series at 1400°C. In the 4-hr experiment (Fig. 2a), the large olivine grains are still angular and only show a limited rounding of their edges: the grain shape of olivine is qualitatively similar to that in the Eagle Station pallasite (Buseck 1977; of course, olivine grain size in our synthetic pallasites is 100 to 1000 times smaller than in real pallasites). On the contrary, the texture in the 7-d experiment (Fig. 2c) is qualitatively similar to textures in pallasites with rounded olivine grains, such as Brenham or Thiel Mountains (except that the volume fraction of olivine is smaller in our experiments than in natural pallasites). The rounding kinetics is very sensitive to both temperature and grain size. The effect of temperature is evident from a comparison of the series at 1200°C and 1400°C: olivine grain shape in the 7-day experiment at 1200°C (Fig. 3c) appears to be roughly equivalent to that in the 4-hr experiment at 1400°C (Fig. 2a). The effect of grain size is clear in Fig. 2c, in which grains less than 5–10 μm in diameter are rounded while larger grains have complex, amoebiform shapes.

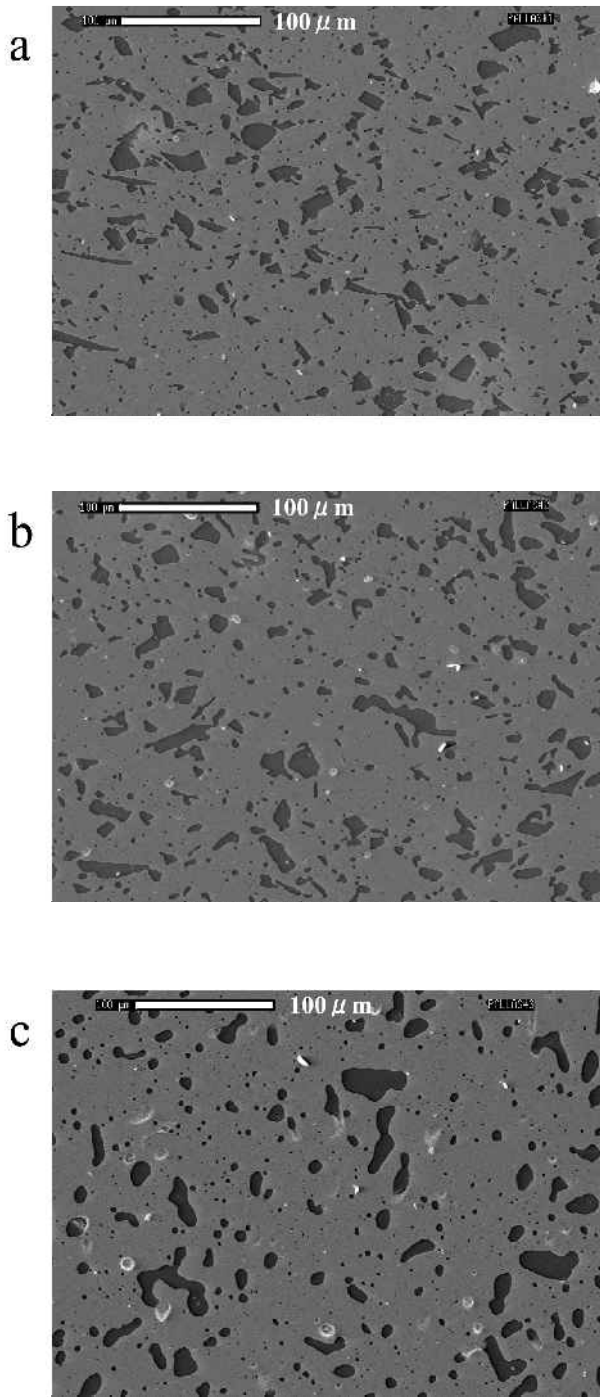


Fig. 2. Secondary electron images of polished sections of the run products at 1400°C. Run duration is: a) 4 hr; b) 27 hr; and c) 7 d. Scale bars = 100 μm .

Reactions Between the Sample and the MgO Container

In all the experiments at $T \leq 1400^\circ\text{C}$, MgO crucibles behaved properly in both chemical and mechanical respects. At 1400°C for instance, the chemical interaction between the sample and the container was restricted to a limited iron

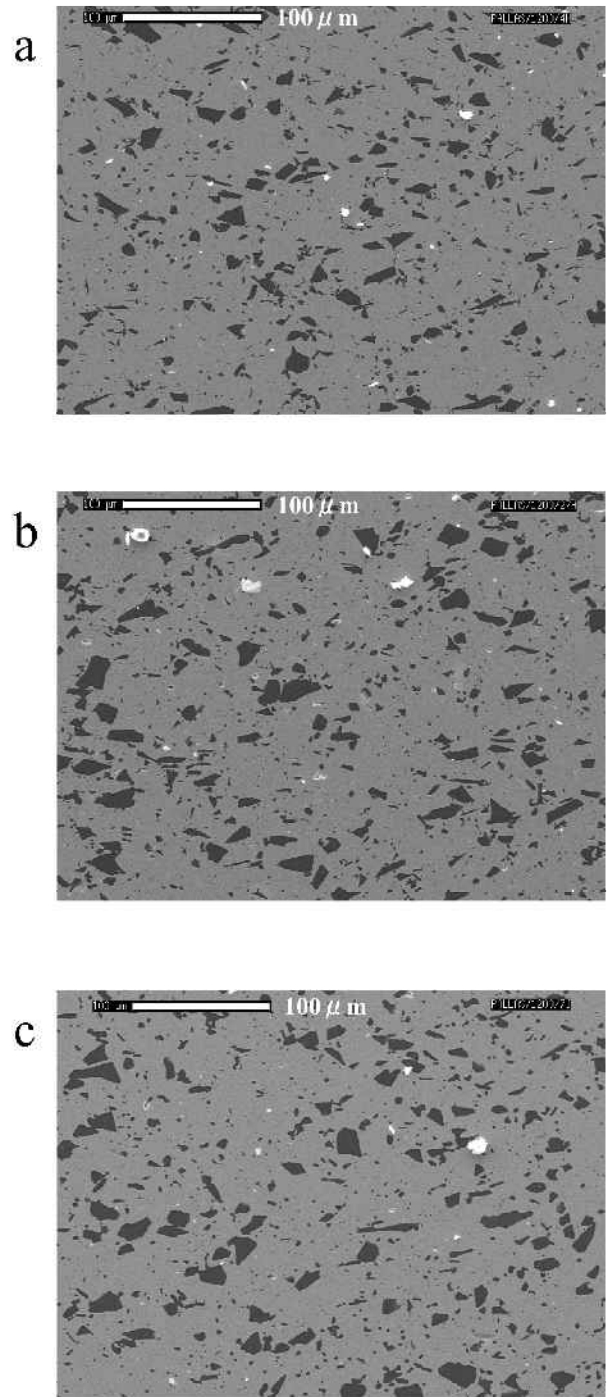


Fig. 3. Secondary electron images of polished sections of the run products at 1200°C. Run duration is: a) 4 hr; b) 27 hr; and c) 7 d. Scale bars = 100 μm .

contamination of the innermost part of the container walls, the Fe/(Fe + Mg) atomic ratio in MgO crystals increasing from zero at 100 μm from the sample, to ≈ 0.1 at the contact with the sample.

Incipient partial melting of the MgO crucible was

observed in the 7-day experiment at 1450°C (Pallas #14; Table 1). In this sample, the MgO lid was crosscut by a number of vertical dikelets, up to 20 μm thick, filled by a mixture of quenched crystals and interstitial melt. This mixture was also found as a discontinuous rim, 40 μm thick at most, separating the sample from the container. Using a defocused beam, we analysed qualitatively the partial melt by energy-dispersive X-ray spectrometry. The spectrum showed a large peak of Mg, smaller peaks of Si and Al, and minor peaks of Fe and Ca. SiO_2 and Al_2O_3 presumably came from the mullite sheath used to host the thermocouple wires. Because the partial melt remained confined at the outside of the olivine-metal sample, the success of Pallas #14 was not compromised.

Olivine Compositions

Olivine compositions were analysed in a few isolated grains in the centre of the experimental samples. Olivines are slightly more iron-rich than the starting olivine (Fig. 4; Table 2) and their compositions do not depend significantly on temperature or run duration. In all the experiments at 1200°C and in the 4- and 27-hr experiments at 1400°C, the olivines show a fairly large compositional dispersion and, usually, faint normal zoning (Fig. 4). For instance, the molar ratio $\text{MgO}/(\text{MgO} + \text{FeO})$ ranges from 0.885 to 0.905 in the 27-hr experiment at 1200°C. By comparison, olivine compositions in the 7-day experiments at 1300°C and 1400°C are more homogeneous.

Reduction of nickel in the olivine is suggested by the drop of the NiO content from 0.3 wt% in San Carlos olivine to about 0.1 wt% at the end of the experiments. We did not observe bright droplets indicative of a metallic phase in the olivine grains, so we suppose that Ni diffused out of the olivine lattices into the metallic matrix.

Morphological Analysis

Two-Dimensional Shape of Olivine Grains

A morphological analysis was performed to characterize quantitatively the evolution of the grain shape of olivine with run duration and temperature. Heywood circular parameter (that is, the ratio of the actual grain perimeter to the perimeter of the circle having the same area as the grain) is generally used to measure grain roundness. This parameter is, however, more sensitive to grain elongation than to roundness. Vector analysis of grain boundaries is also not fully satisfying because, at the pixel scale, the boundary vector can only take eight directions (0° , 45° , 90° , 135° , 180° , -45° , -90° , and -135°). To measure the roundness of olivine grains, Saiki (1997) developed a technique in which the grain outline was fitted by a spline curve. The curvature was then computed all along the outline and the degree of grain roundness was estimated by calculating the standard deviation of curvature. In this technique, the pixels making the grain outline must be reduced to punctual

nodes before spline fitting, and the final results depend somewhat on where the nodes are located within the original pixels. Also, small scale features, such as an angular corner, can vanish during the pixel-to-node transformation.

To overcome these drawbacks, a new image analysis procedure referred to as the ‘‘Gaussian Diffusion-Resample’’ method (GDR method) was developed. The reason that the human brain can detect small variations in roundness is its ability to change the scale of observation. The GDR method incorporates a scale change routine for the measurement of grain roundness. It is similar to fractal analyses, such as the boxcounting method, but is more sensitive to roundness.

The GDR method involves the following steps (Fig. 5): 1) binarize an image of a polished section of the synthetic pallasite; 2) pick up twenty large, isolated grains and make a new representative image containing the selected grains (in our standard procedure, the size of the grains considered for morphological analysis were about 20–60 pixels long, that is, 10–30 μm long); 3) measure the total area of grains; 4) filter the image using a gaussian diffusion filter (see below) with an aperture equal to half a pixel; 5) resample the image, that is, rebinarize the image using a threshold of grey level such that the total area of grains in the rebinarized image and in the initial image are equal; 6) subtract the rebinarized image from the initial image to materialize the portions of the grains that are consumed (‘‘eroded’’) in the diffusion-rebinarization steps; 7) count the eroded area; and 8) increase the aperture of the gaussian diffusion filter and repeat steps 4 to 7. The source of the macro program used to implement the GDR method is given in the appendix.

A gaussian filter carries out gaussian distribution diffusion of the value of the pixel of an original image. In the binary image, black and white pixels are set to 255 and 0, respectively. A surrounding pixel is made by diffusing this numerical value of 255. The distributions before and after gaussian diffusion are shown in Fig. 6. Although the example of Fig. 6 is one-dimensional, pixel value is diffused in two dimensions in practice. The matrix of the two-dimensional Gaussian distribution used for diffusion process is shown in the macro code. The aperture of a gaussian filter is defined as the value of standard deviation (one sigma) of the gaussian distribution. The pixel of an original image spreads more widely when the aperture of the gaussian filter is larger. Gaussian diffusion followed by rebinarization makes the grains rounder (Fig. 5c). The resampling process is explained in Fig. 7, using a one-dimensional case. An original line comprising five black pixels (Fig. 7a) is first transformed by gaussian diffusion to produce the distribution of grey levels shown in Fig. 7b. The pixel line is then rebinarized using a threshold value of grey level such that the number of black pixels after resampling (Fig. 7c) is equal to 5 as in the original line (Fig. 7a). Through the GDR process, the hole on the right in the original line (Fig. 7a) has been filled and the isolated point on the left has vanished. Therefore, the GDR process acts

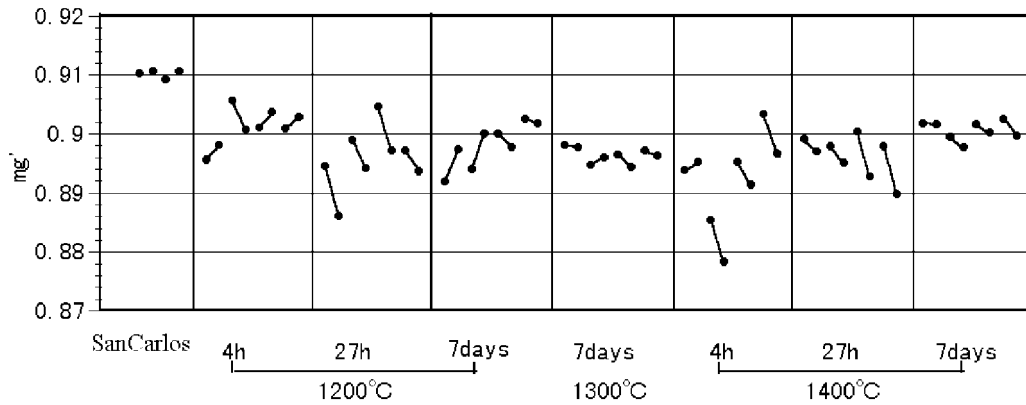


Fig. 4. Olivine compositions in the run products; mg' is the molar ratio $MgO/(MgO + FeO)$. Connected points correspond to analyses made in a single grain (core composition is on the left, rim composition is on the right). The composition of San Carlos olivine is shown for comparison.

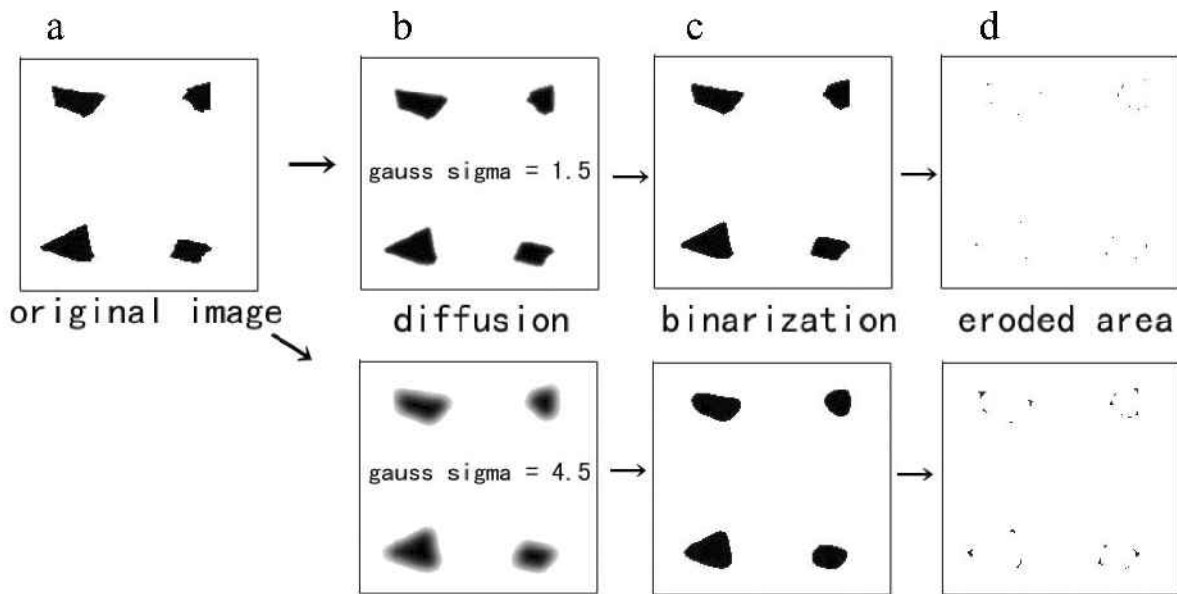


Fig. 5. The Gaussian Diffusion-Resample method: a) initial image constructed by picking up twenty large grains from the binarized secondary electron image (for clarity, only four grains are shown); b) image filtered by Gaussian diffusion; c) rebinarized image; the total area of grains in the initial image and in the rebinarized image are equal; and d) resultant image obtained by subtracting (c) from (a). The subtraction in (d) yields a few islands of residual pixels for each grain that correspond to the angular portions of the olivine grains. The aperture of the Gaussian diffusion filter is 1.5 pixels in the upper row and 4.5 pixels in the lower row.

qualitatively like Ostwald ripening, a process in which matter is transported from the small grains in a suspension to the large grains.

The subtraction of the resampled image from the initial image yields a few islands of residual pixels for each grain that correspond to the angular portions of the olivine grains (Fig. 5d). After each increment of the aperture of the Gaussian diffusion filter, the islands increase in size. That is, the portions of grains eroded in the GDR process increase (compare the upper and lower row in Fig. 5). Eroded areas in step (7) are measured in pixels. We used a normalization procedure in which, for each grain, the eroded area was

divided by the grain perimeter in the initial binary image (the perimeter is the number of pixels that define the grain outline in the binary image). The smaller the normalized eroded area of a grain, the more rounded the grain.

For each representative image, we computed the sum EA of the normalized eroded area of the twenty grains as a function of filter aperture (in pixel, the typical size of a pixel being equal to $0.5208 \mu\text{m}$). Plots of EA versus filter aperture for the kinetic series at 1200°C , 1300°C , and 1400°C are shown in Figs. 8a, b, and c, respectively; the results for the 7-day experiments at 1200°C to 1450°C are plotted in Fig. 8d. For a given experiment, that is, for a given initial binary

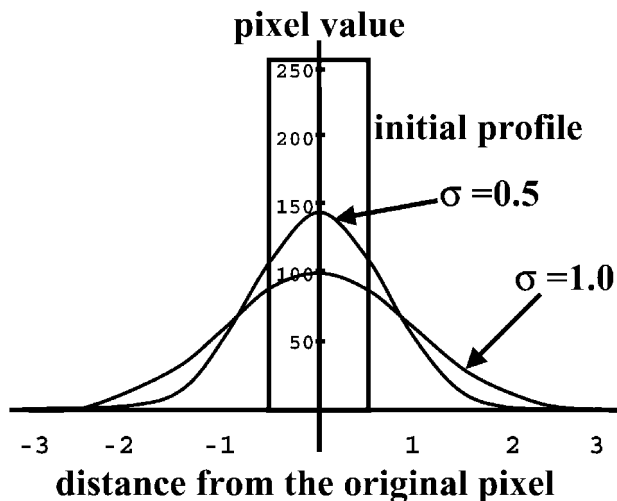


Fig. 6. Sketch showing one-dimensional Gaussian diffusion.

image, EA rapidly increases with increasing filter aperture (the increase is almost linear if the data for filter apertures ≤ 1 pixel are not taken into account). The very contrasted degrees of grain roundness observed in the experimental textures (Figs. 2 and 3) are obvious in Fig. 8. For a given filter aperture, the value of EA is smaller in an experiment with more rounded grains than in an experiment with less rounded grains. As a result, the slope of the EA filter aperture plot decreases with increasing grain roundness. The effect of run duration on grain roundness is well illustrated in Figs. 8a–c. For a given filter aperture and temperature, the total eroded area is larger in the 4-hr experiment and smaller in the 7-day experiment (see, for instance, the kinetic series at 1400°C; Fig. 8c). The effect of temperature is displayed in Fig. 8d, in which the total eroded area seems to decrease continuously with temperature increasing from 1200°C to 1450°C (this effect is best visible at large filter apertures).

To study the effect of grain size on the rounding process, the roundnesses of small grains, $\approx 2.4\text{--}7.1\ \mu\text{m}$ long, in the 4-hr experiments at 1200°C, 1300°C, and 1400°C were measured and compared with the roundnesses of the large grains. The twenty small grains were picked up from a SEM image at a larger magnification and had an average area (in number of pixels) approximately equal to the average area of the twenty large grains used for morphological analysis in our standard procedure. Therefore, the small grains and the large ones were treated at almost the same spatial resolution. The pixel size for the large grains ($0.5208\ \mu\text{m}$) was 4.38 times the pixel size for the small grains ($0.119\ \mu\text{m}$). Taking into account the fact that the grains analyzed did not all have exactly the same area, the small grains were 4 to 5 times smaller than the large grains.

The small grains in the three 4-hr experiments are much more rounded than the large grains (Figs. 8a–c). In fact, the degree of roundness of the small grains in a 4-hr experiment is

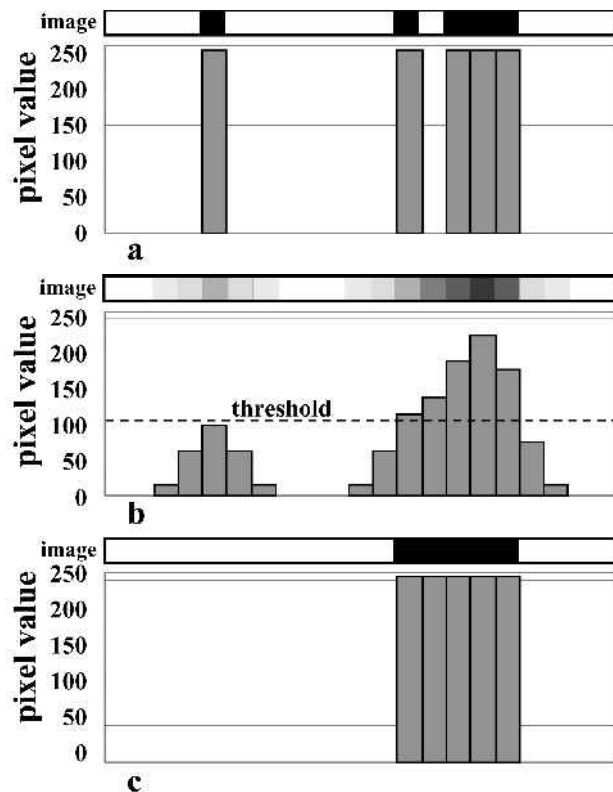


Fig. 7. Application of the GDR method to a binary line comprising 5 black pixels: a) distribution of gray levels in the initial binary image; b) distribution of gray levels after gaussian diffusion; and c) distribution of gray levels after resampling. The threshold value used in the resampling stage is shown by the dashed line in (b). It is chosen such that the numbers of black pixels in the final binary line is equal to 5, as in the initial line.

equal to or just slightly larger than the degree of roundness of the large grains in the 7-day experiment at the same temperature (for instance, Fig. 8c). This observation can be used to constrain the rounding kinetics of olivine. As explained in the Discussion section, the time scale of rounding, τ , depends on grain radius, R , according to a law of the form:

$$\tau \propto R^n \quad (1)$$

A fundamental parameter of the kinetic law is the exponent n , which is especially important when the experimental data are to be extrapolated to time scales several orders of magnitude longer than the experimental time scales. If we assume that the small grains in the 4-hr experiments and grains about 4.4 times larger in the experiments lasting 168 hr are equally rounded, we can write the relation:

$$\left(\frac{168}{4}\right) \approx \left(\frac{4.4R}{R}\right)^n \quad (2)$$

from which we compute $n \approx 2.5$. In fact, the value of n must be closer to 3 because, at all three temperatures investigated,

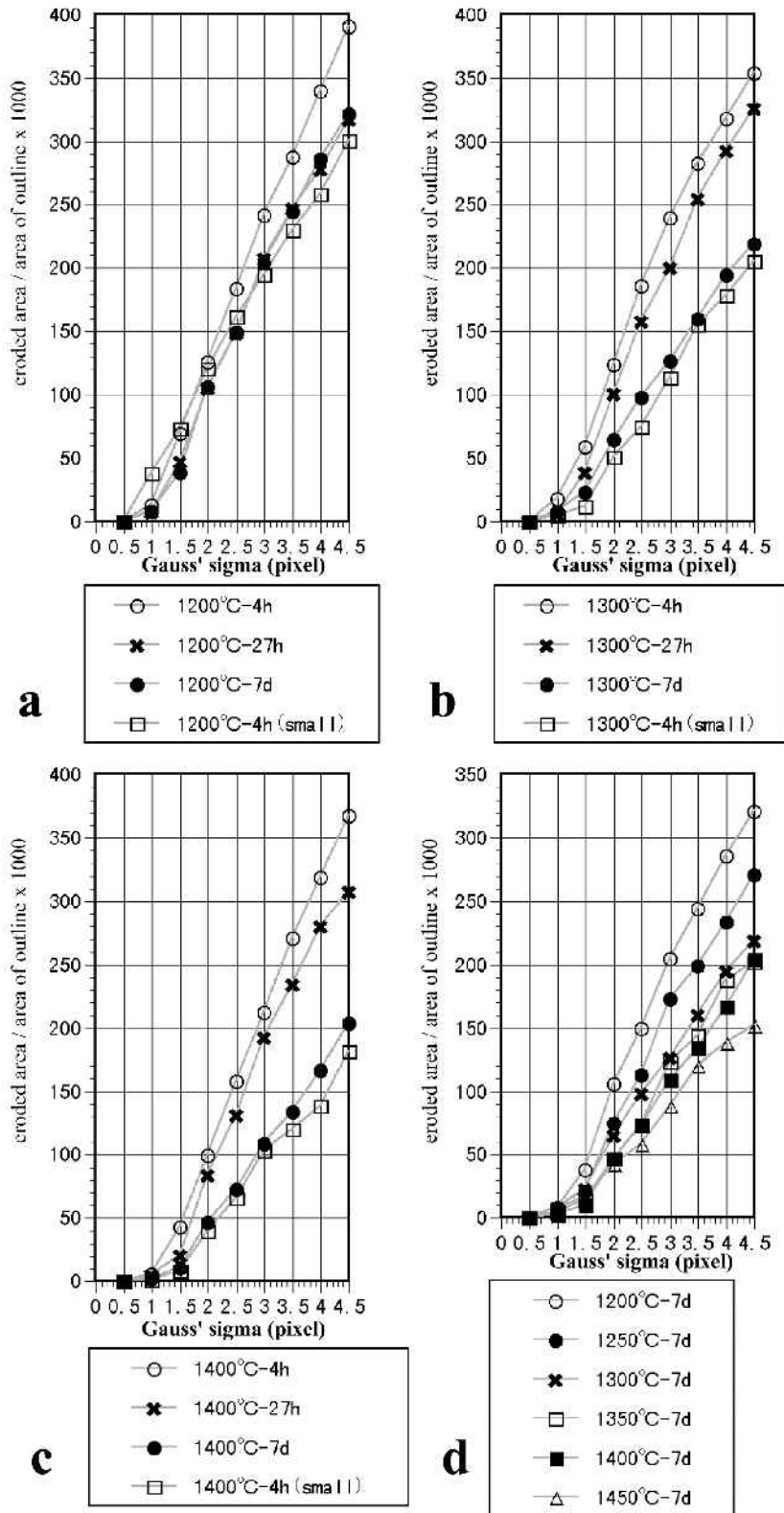


Fig. 8. Normalized eroded areas as a function of filter aperture, in pixels, for: a) 1200°C time series; b) 1300°C time series; c) 1400°C time series; and d) 7-day experiments. In (a)–(c), the normalized eroded areas for small grains in the 4-hr experiments are shown for comparison (see text for further explanation).

the small grains are slightly more rounded than the large grains (Figs. 8a–c).

Three-Dimensional Shape of Olivine Grains

Polished sections of the experimental samples were etched with nital to reveal the 3-D shape of the olivine grains. The 3-D textures observed in sample Pallas #3 (1400°C, 7 days; Table 1) are illustrated in Fig. 9. In the etched sections, the large grains show irregular shapes and commonly occur as clusters (Figs. 9a–b). In contrast, the small grains are ovoid to nearly spherical (Fig. 9c). In detail, the surface of the large grains is not smoothly curved: we see curved edges separating slightly concave faces (Figs. 9a–b). Edges and faces are also observed in the smaller grains but the faces are subplanar to

slightly concave. By analogy with the equilibrium texture of polycrystalline aggregates (e.g., Smith 1964), the olivine faces in Fig. 9 are presumed to correspond to the boundaries between an olivine grain and a metal grain, and the edges are the junction lines where an olivine grain and two metallic grains were in contact. From the size of the olivine faces in Figs. 9a–b, we infer that the Fe-Ni grains in the metallic matrix are a few μm to a few tens of μm in size.

At first approximation, the olivine grains in our experiments can be divided in two groups: small, spherical grains and large, irregularly-shaped grains. On the basis of this observation, it is possible to define, for a given experiment, the critical diameter D_C of the olivine grains in a given experiment as the diameter above which a grain cannot

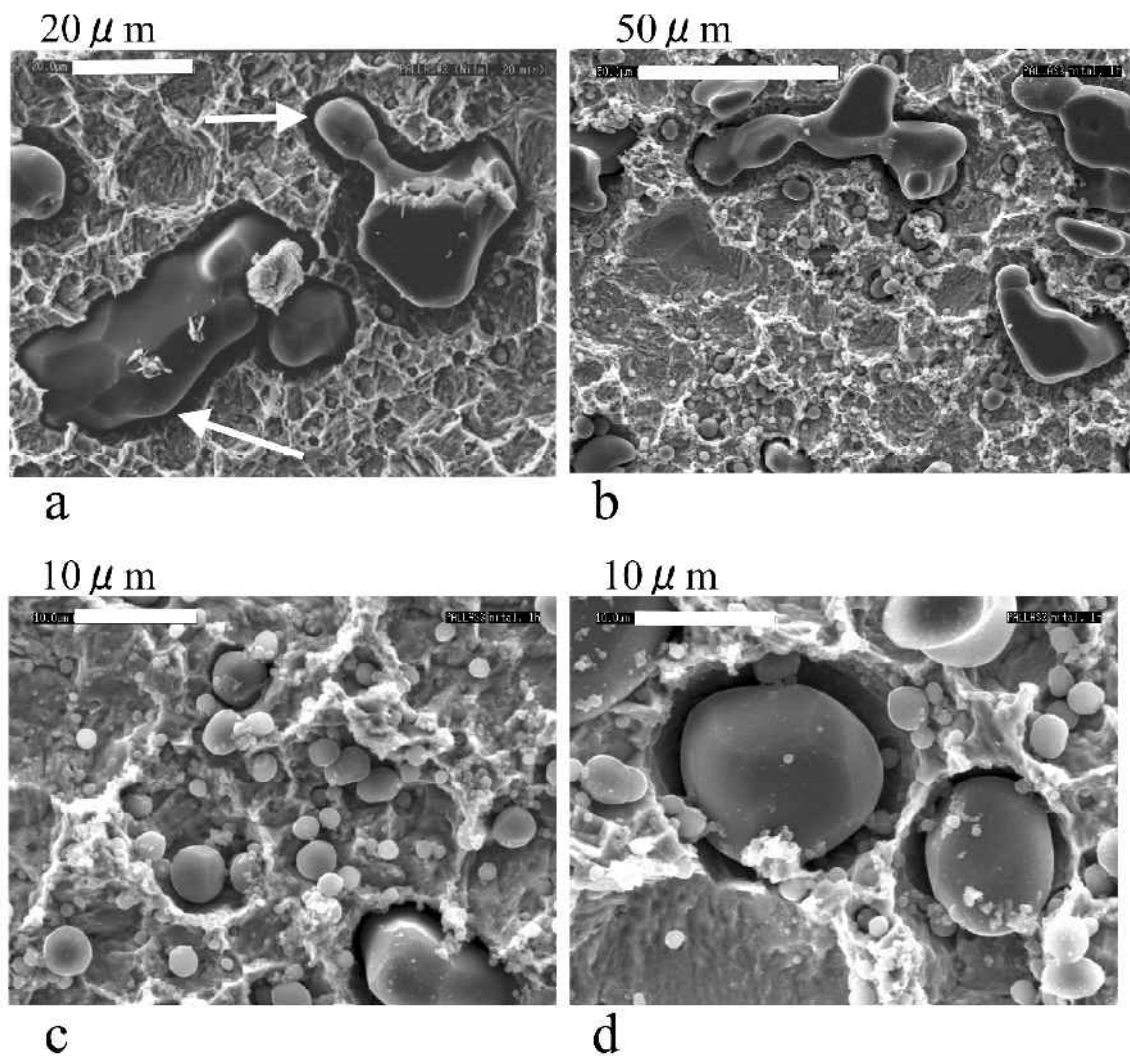


Fig. 9. Secondary electron images of a polished section of sample #3 (1 GPa, 1400°C, 7 days) after etching with nital to reveal the 3-D shape of olivine grains: a) and b) overviews showing clusters of large, irregularly-shaped grains and small, more rounded grains; note the curved edges on the surfaces of the large olivine grains (arrows); c) close-up of (b) showing the rounded shape of the small grains; and d) a view of the largest, nearly spherical olivine grain found in sample #3 ($D_C = 13.9 \mu\text{m}$).

get rounded to a sphere within the time scale of the experiment. With the SEM, we surveyed the etched section of most samples looking for the largest, nearly spherical grain (as emphasized above, the olivine grains are never perfectly spherical because they are embedded in a polycrystalline matrix which is not in an isotropic medium like a fluid phase; Fig. 9d). The measurement of critical diameters is not very accurate because it relies on a visual estimate of sphericity. However, in all samples, we were able to find several large, nearly spherical grains with a diameter equal to or just slightly smaller than D_C . Our measurements are reported in Table 1; the accuracy is estimated to range from 10% for the large values of D_C (17.1 μm in Pallas #14 [168 hrs at 1450°C]) to 20% for the small values of D_C (<2 μm in Pallas #7 [4 hrs at 1200°C]).

To compare our two techniques of morphological analysis, we computed the value EA^* of the normalized eroded area for a filter aperture of 3.5 pixels (we chose a large filter aperture because it allows a better discrimination of the samples; see Fig. 8), and we plotted the critical diameter as a function of EA^* (Fig. 10a). The good negative correlation between D_C and EA^* shows that these parameters provide two independent but concordant estimates of the degree of textural maturity. For a given run duration, D_C increases and EA^* decreases progressively with increasing temperature (Fig. 10a). For a given temperature, D_C increases and EA^* decreases with increasing run duration. To better constrain the kinetics of rounding, the critical diameters were plotted as a function of run durations for the three series at 1200°C, 1300°C, and 1400°C (Fig. 10b). In a diagram $\log(D_C)$ - $\log(t)$, the three series yield subparallel trends with slopes of 0.30 at 1300°C and 1400°C, and 0.27 at 1200°C. The effect of temperature on the critical diameters is important: at 1200°C, D_C increases from ≈ 1.6 μm at $t = 4$ hrs to 4.3 μm at $t = 168$ hrs; at 1400°C, the critical diameter is equal to 4.5 μm at $t = 4$ hrs and it reaches 13.9 μm at $t = 168$ hrs.

DISCUSSION

Kinetics of Olivine Rounding: Theory

We succeeded in reproducing the textural features of pallasites at a miniature scale. The rate of rounding was fast enough to be observed over time scales of a few hours to a few days, even though our experiments were performed below the solidus of the Fe-Ni metal. Grains ≤ 14 μm in diameter become nearly spherical within 7 days at 1400°C. This rate is at least 1000 times more rapid than the value predicted by Ohtani (1983) for solid-state diffusion. In order to apply our data to natural pallasites, the effects of temperature, pressure, and grain size on the kinetics of rounding must be known. The experimental pressure (1 GPa) is larger than the pressure prevailing in pallasite parent bodies. The pressure at the center of a parent body 20 to 50

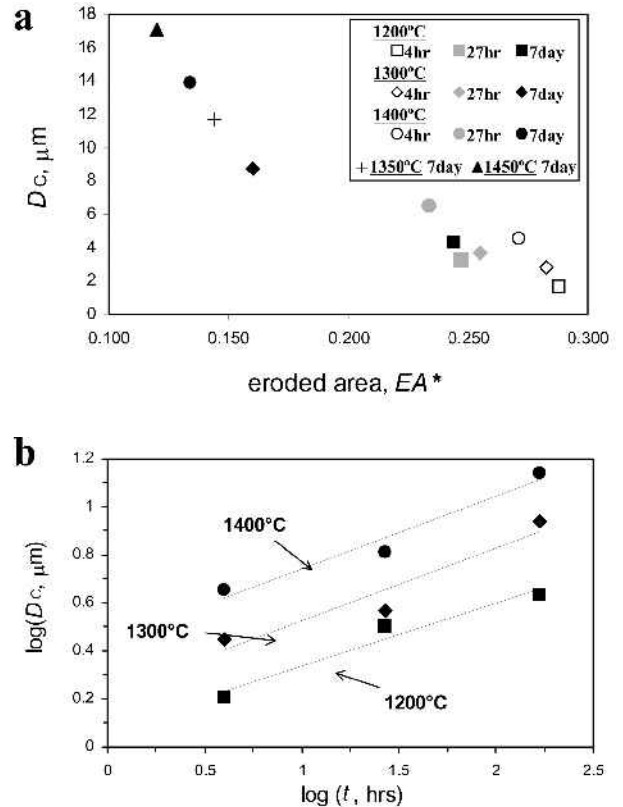


Fig. 10. a) Critical diameter D_C (μm) versus the eroded area EA^* (EA^* is the eroded area computed for a filter aperture of 3.5 pixels). The data points at 1200°C, 1300°C, and 1400°C are plotted as squares, diamonds, and circles, respectively. The empty symbols correspond to the 4-hr experiments, the grey symbols to the 27-hr experiments, and the filled symbols to the 7-day experiments. The 7-day experiments at 1350°C and 1450°C are shown by the cross and the filled triangle, respectively. b) Critical diameters (μm) as a function of run durations (hr) for the series at 1200°C (squares), 1300°C (diamonds), and 1400°C (circles). The best linear fits are: $\log(D_C) = 0.301 \log(t) + 0.443$ at 1400°C; $\log(D_C) = 0.302 \log(t) + 0.223$ at 1300°C; $\log(D_C) = 0.265 \log(t) + 0.071$ at 1200°C.

km in diameter must be of the order of 1 MPa and the pressure of a parent body 600 km in diameter is about 150 MPa. However, the physical parameters controlling the rounding kinetics of olivine in solid FeNi metal, such as the olivine-metal interfacial energy and the diffusion coefficients of the olivine components, are not critically dependent upon pressure. Therefore, we believe that the effect of pressure is minor compared to the effect of temperature or grain size.

To discuss the effect of grain size, we assume that each grain of olivine behaved as an isolated system during the course of an experiment. The grain's shape evolved to reduce its total interfacial energy, but its volume remained constant. In other words, interfacial energy was minimized only or mostly through changes in the shape of the olivine grains, not through changes in grain size, as in Ostwald ripening. When Ostwald ripening is active, its most visible effects are an

increase of the average grain size, a decrease of the frequency of small grains, and a strong decrease of the number of grains per unit volume (e.g., Cabane, Laporte, and Provost 2001). None of these effects was observed in our experiments (compare Figs. 2a and 2c), so we can reasonably neglect Ostwald ripening.

Because of the very low solubility of olivine components in solid metal (which explains why Ostwald ripening is negligible in our experiments), the rounding of the edges of an olivine grain embedded in a solid Fe-Ni matrix is thought to occur either by surface diffusion of matter along the olivine-metal interface or by volume diffusion in the olivine lattice. Therefore, the rounding process may be compared to deformation by diffusion creep (e.g., Poirier 1985), in which matter is transported either within the crystal lattice (Nabarro-Herring creep; Herring 1950) or along grain boundaries (Coble creep; Coble 1963). The main difference between diffusion creep and the rounding process is the driving force. Diffusion creep operates when a grain is placed in a non-hydrostatic stress field so that grain boundaries with different orientations are subjected to different stresses. In the rounding process investigated in this study, the driving force is the minimization of the interfacial energy of an olivine fragment embedded in a metallic matrix. Gradients in interfacial curvature along the olivine-metal interface produce chemical potential gradients which drive a flux of matter from regions of larger curvature, such as edges and corners, to regions of smaller curvature, such as the faces of the olivine fragment. Ultimately, the olivine fragment should reach an equilibrium shape with a constant mean curvature. We assume that the olivine-metal interfacial energy per unit area γ (J m⁻²) is isotropic, i.e., the coefficient γ does not depend on the orientation of the olivine-metal interface relative to the olivine or metal crystalline lattices. In the discussion below, we consider that the basic unit of matter in the diffusion process is an olivine molecule. This is based on the multicomponent diffusion model of Jaoul (1990), in which the fluxes of individual species (Si⁴⁺, Mg²⁺, Fe²⁺, O²⁻) are coupled so that they all move with the same velocity and the stoichiometry of olivine is preserved during transport.

The relationship between the chemical potential of olivine μ (J) and the mean curvature of the olivine-metal interface, κ (m⁻¹), is given by the Gibbs-Thompson equation (Shewmon 1963).

$$\mu = \mu_0 + \Omega\gamma\kappa \quad (3)$$

where μ_0 is the chemical potential for a flat interface and Ω (m³) is the molecular volume of olivine. The chemical potential gradient that is associated with a variation of mean curvature along the olivine-metal interface is responsible for a flux of olivine molecules, as sketched in Fig. 11. The flux along the x-axis is expressed as (e.g., Bějina, Jaoul, and Liebermann 1999):

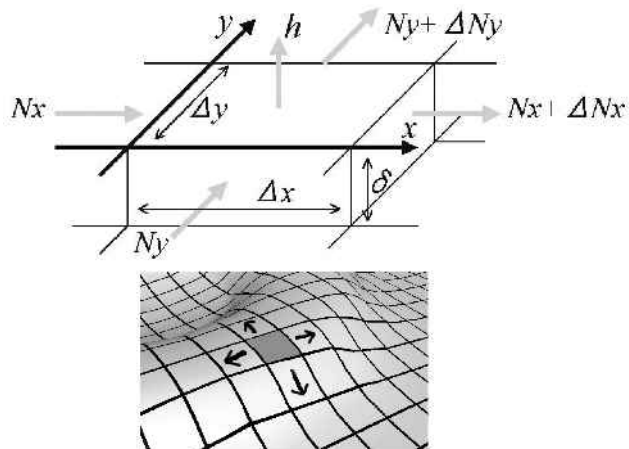


Fig. 11. Sketches showing the model for matter transport near the surface of olivine grains. Gradients in chemical potential along the olivine-metal interface drive a flux of olivine molecules from regions of larger curvature, such as the hump in the bottom sketch, to regions of smaller curvature. The main variables used in the text are defined in the upper sketch.

$$J_x = -\frac{D}{kT\Omega} \frac{\partial \mu}{\partial x} \quad (4)$$

where J_x (s⁻¹m⁻²) is the number of molecules flowing through a 1 m² section normal to x-axis per second, D (m²s⁻¹) is the diffusion coefficient of olivine either within the crystalline lattice or in the grain boundary (see below), k is the Boltzmann constant (J K⁻¹), T (K) is the temperature, and x (m) is a distance along the interface. The flux of molecules along the y-axis, J_y , can be expressed in the same way. The magnitude of J changes along the olivine-metal boundary due to variations of the interfacial curvature. In turn, these changes in magnitude produce local changes in the volume and shape of the olivine grain along its interface. Let ΔN be the variations of the number of molecules in a small interfacial region of edge lengths Δx and Δy during a short time interval Δt (Fig. 11):

$$\Delta N = -\left(\frac{\partial N_x}{\partial x} \Delta x + \frac{\partial N_y}{\partial y} \Delta y\right) \Delta t \quad (5)$$

Using Equation 4, N_x and N_y can be expressed as follows:

$$N_x = -\frac{D}{kT\Omega} \frac{\partial \mu_x}{\partial x} \Delta y \delta \Delta t \quad (6)$$

$$N_y = -\frac{D}{kT\Omega} \frac{\partial \mu_y}{\partial y} \Delta x \delta \Delta t \quad (7)$$

where δ (m) is the effective thickness of the diffusion path (see below). Substituting Equations 6 and 7 in Equation 5, we get:

$$\Delta N = \frac{D}{kT\Omega} \left(\frac{\partial^2 \mu_x}{\partial x^2} + \frac{\partial^2 \mu_y}{\partial y^2} \right) \Delta x \Delta y \delta \Delta t \quad (8)$$

Since ΔN causes a volume change ΔV , ΔN can be written:

$$\Delta N = \frac{\Delta V}{\Omega} = \frac{dh}{dt} \Delta t \frac{\Delta x \Delta y}{\Omega} \quad (9)$$

where h (m) is the height of the small element of the olivine surface (Fig. 11).

Using Equations 3, 8, and 9, we finally obtain:

$$\frac{dh}{dt} = \frac{D}{kT} \left(\frac{\partial^2 \kappa_x}{\partial x^2} + \frac{\partial^2 \kappa_y}{\partial y^2} \right) \gamma \Omega \delta \quad (10)$$

This relation shows that the rate of rounding depends highly on the local grain shape, as embodied by the curvature term κ_x, κ_y . In particular, the rate of rounding is fast where a large variation of the curvature gradient occurs over a short distance, such as at a sharp edge.

We stress that Equation 10 can be used for both surface and volume diffusion except that the values of D and δ must be different in both cases. In particular, δ will be critically dependent on the diffusion model. In the case of surface diffusion, δ is related to the thickness of the grain boundary (that is, it is equal to a few interatomic distances) and is therefore independent on grain size. In the case of volume diffusion, the diffusion geometry is supposed to be more complex and to depend on grain shape, but we may anticipate that the thickness of the diffusion path scales to the grain size (similarly, the thickness of the diffusion path is considered to be of the order of the grain radius in the case of Nabarro-Herring creep). This contrasted behavior of δ leads to major differences in rounding kinetics, as discussed in the next section.

Kinetics of Olivine Rounding: Experimental Constraints

Our rounding experiments were performed with olivine grains less than 20 μm in size to accelerate the rate of rounding. Olivine grain sizes in pallasites with rounded olivines are typically in the range of 5–15 mm (Scott 1977b). Therefore, a scale change by a factor up to 750 is required to apply the experimental data to natural pallasites. To evaluate the effect of this scale change on the time scale of rounding, we rearrange Equation 10 as follows:

$$\Delta t = \frac{kT}{D\gamma\Omega\delta} \left[\frac{\partial^2 \kappa_x}{\partial x^2} + \frac{\partial^2 \kappa_y}{\partial y^2} \right]^{-1} \Delta h \quad (11)$$

where Δt is the time required to produce a variation Δh of the height of a small element of the olivine interface. Consider two grains of similar shape but with different sizes: grain No. 2 is s times bigger than grain No. 1. For grain No. 1, a variation of height Δh_1 is produced in a time Δt_1 . Now, we need to compute the time Δt_2 required to produce the same relative shape transformation in grain No. 2 (that is, $\Delta h_2 = s \cdot \Delta h_1$). If grain size is multiplied by s , then all radii of curvature are

multiplied by s and the second derivatives of curvature in Equation 11 are multiplied by s^{-3} . In the case of surface diffusion, the thickness of the diffusion path is independent of grain size, so finally, a scale change by a factor s results in a factor s^4 increase in Δt : $\Delta t_2 = s^4 \cdot \Delta t_1$. On the contrary, in the case of volume diffusion, δ is proportional to grain size so that a scale change by a factor s results in a factor s^3 increase in Δt : $\Delta t_2 = s^3 \cdot \Delta t_1$. Accordingly, the time scale of rounding, τ , of an olivine grain of radius R must be of the form:

$$\tau \propto \frac{R^4}{\gamma \delta_{gb} D_{gb}} \quad (12)$$

in the case of surface diffusion (D_{gb} is the grain-boundary diffusion coefficient and δ_{gb} is the thickness of a grain boundary), and of the form

$$\tau \propto \frac{R^3}{\gamma D_v} \quad (13)$$

in the case of volume diffusion (D_v is the volume diffusion coefficient). In both cases, τ decreases with decreasing grain size and with increasing diffusion coefficient or interfacial energy but the grain-size dependence is stronger in the case of surface diffusion. In his theoretical study of the rounding of olivine grains in a metallic matrix, Ohtani (1983) already reported kinetic laws in R^4 for surface diffusion and in R^3 for volume diffusion. Relaxation time scales proportional to R^4 were also reported by Toriumi (1979) and Kern (1987) for the rounding of small crystals by surface diffusion.

It is interesting to note that the powers of R in the kinetic laws (12) and (13) are different from those derived for diffusion creep. In diffusion creep, the strain rate $\dot{\epsilon}$ is given by the following relations (Poirier 1985):

$$\dot{\epsilon} \propto \frac{\sigma \delta_{gb} D_{gb}}{R^3} \quad (14)$$

in the case of surface diffusion (Coble creep; σ is differential stress), and

$$\dot{\epsilon} \propto \frac{\sigma D_v}{R^2} \quad (15)$$

in the case of volume diffusion (Nabarro-Herring creep). Obviously, these differences are due to the different driving forces involved. Basically, the rounding of an olivine grain occurs in response to gradients in capillary pressure which result from gradients in curvature along the olivine-metal interface. As in the case of an interface between two immiscible fluids, capillary forces acting along a curved interface in a polycrystalline material give rise to capillary pressures which tend to move any element of the interface normal to itself (e.g., Sutton and Balluffi 1995, p. 379). The capillary pressure writes:

$$\Delta P = \gamma \kappa = \gamma \left(\frac{1}{r_1} + \frac{1}{r_2} \right) \quad (16)$$

where κ is the local mean curvature of the element of interface and r_1 and r_2 are its two principal radii of curvature. From Equation 16, we see that, when grain size is multiplied by a factor s (at constant grain shape), then the capillary pressure anywhere along the interface is divided by s . Accordingly, the driving force of the rounding process is proportional to γ but inversely proportional to grain size. This is a major difference with diffusion creep, in which the stress difference between two faces of a grain only depends on the orientation of the two faces relative to the non-hydrostatic stress field, not on grain size. Now, if we replace the stress σ in Relations 14 and 15 by a pressure term proportional to γ/R , we obtain kinetic laws in γ/R^d and γ/R^3 , in agreement with Relations 12 and 13, respectively.

The experimental textures in our study were characterized quantitatively using two independent analytical techniques that both point to a value of n closer to 3 than to 4. First, a value of n slightly larger than 2.5 was inferred from the morphological comparison between the small grains in the 4-hr experiments and the large grains in the 7-day experiments at the three temperatures investigated. Second, the increase of the critical diameter with increasing run duration at 1300°C and 1400°C corresponds to an exponent $n \approx 3.3$. On the contrary, the slope of the $\log(D_c)$ - $\log(t)$ plot for the time series at 1200°C yields an exponent n close to 4 (≈ 3.8). This larger value of n could result from a switch of the dominant diffusion mechanism from volume diffusion at high temperatures to surface diffusion at 1200°C. An exponent $n = 4$ is not in agreement, however, with the rate of rounding deduced from the comparison of the small grains in the 4-hr experiment at 1200°C and the large grains in the 7-d experiment at 1200°C. For $n = 4$, it should indeed take more than 1000 hr for grains of radius $4R$ to become as rounded as grains of radius R in a 4-hr experiment. In fact, the smaller slope at 1200°C in Fig. 10b may not be meaningful. If the critical diameter in the 4-hr experiment at 1200°C is changed to 1.4 μm instead of 1.6 μm (which is well within the measurement error), then the slope increases to 0.30. Accordingly, we conclude that the changes in grain shape in all our experiments occurred predominantly by volume diffusion in the olivine crystalline lattices, not by surface diffusion along the olivine-metal boundaries.

Implications for the Thermal History of Pallasites

Our experimental results can be used to estimate the time scales required for rounding large olivine grains, up to 10–15 mm in size, in a solid Fe-Ni matrix. Our estimations of the rounding time scales, τ , for olivine grains of radius $R = 0.1$ mm and 5 mm are reported in Table 3. The calculations were made for temperatures of 1400°C, 1300°C, and 1200°C,

Table 3. Time scales of rounding of olivine grains of 0.1 mm and 5 mm radius.^a

	n = 3			n = 4
	1400°C	1300°C	1200°C	1400°C
R = 0.1 mm	57 a	233 a	1928 a	825 a
R = 5 mm	7 Ma	29 Ma	241 Ma	5100 Ma

^aThe time, τ , required for rounding an olivine grain of radius R was computed using the relation: $(\tau/\tau_{\text{ref}}) = (2R/D_{\text{ref}})^n$, with $n = 3$ or 4, and $\tau_{\text{ref}} = 7$ days. D_{ref} is equal to the critical diameter measured in the 7-day experiments: 13.9 μm , 8.7 μm , and 4.3 μm at 1400°C, 1300°C, and 1200°C, respectively (Table 1).

taking $n = 3$ in kinetic law (1). For comparison, τ was also computed for $n = 4$ and $T = 1400^\circ\text{C}$.

Scott (1977b) observed that the large angular grains of olivine in the Eagle Station pallasite (Fig. 1b) had rounded grain edges and that the small olivine grains, a few hundreds of μm in diameter, were well rounded. These textural features were the best evidence to claim for a high-temperature annealing stage in the formation of pallasites. The origin of these features can be discussed on the basis of the time scales computed for $R = 0.1$ mm in Table 3. The most important implication of our experimental study is to show that small scale rounding of olivine grains in a solid metal matrix can be produced within relatively short time intervals: ≈ 100 yr for $R = 0.1$ mm at 1300–1400°C (for $n = 3$). For $n = 4$, τ is longer but remains lower than 10^3 yr (Table 3). Accordingly, the very limited rounding of olivine grain edges in pallasites such as Eagle Station requires a rapid cooling after olivine-metal mixing. This result is in good qualitative agreement with the shallow burial depth deduced by Miyamoto (1997) from concentration profiles in olivine. A low to moderate burial depth for pallasites is in apparent contradiction with a provenance from the core-mantle boundary. One way to reconcile these two points of view is to assume that the silicate mantle was almost totally excavated by the impact that was responsible for olivine fragmentation and olivine-metal mixing.

Scott's (1977b) model provides a convincing scenario for the formation of pallasites with angular olivines. Scott argued that his model can also account for the formation of pallasites with large rounded grains of olivine, 5–15 mm in diameter, such as Brenham (Fig. 1a). A longer stage of high-temperature annealing (or a larger amount of sulfide liquid trapped in the pallasite; see below) would be responsible for the development of near-equilibrium olivine-metal textures in these pallasites. The calculations for $R = 5$ mm in Table 3 show that the time scales required to make large, rounded olivine grains by annealing in a solid metallic matrix at 1200–1400°C are of the order of 10 to 100 Ma. Considering that the time interval for partial melting, differentiation and solidification of pallasite parent bodies is ≈ 20 Ma (Shen, Papanastassiou, and Wasserburg 1998), we conclude that the large, rounded grains in Brenham-type pallasites cannot be produced by annealing olivine fragments in a solid Fe-Ni

matrix. This result is a strong argument in favor of the hypothesis that pallasites are igneous cumulates, as proposed by Wood (1978), Takahashi (1983), and Greenberg and Chapman (1984). However, we cannot definitely exclude that large, rounded grains of olivine in pallasites were formed from fragments by high-temperature annealing (Scott 1977b; Wasson et al. 1999), because our experiments do not document the effect of sulfur on the rounding kinetics. A pallasite with a typical troilite content of 1 wt% would contain $\approx 5\%$ of sulfide liquid at 1400°C, and sulfide liquid will coexist with olivine and solid metal down to $\approx 1000^\circ\text{C}$ (the eutectic temperature in the Fe-Ni-S system; Urakawa, Kato, and Kumazawa 1987). Ohtani (1983) suggested that the presence of a sulfide melt film around the olivine grains could reduce dramatically the time scale of rounding, but this result has not yet been confirmed experimentally.

To conclude, an important implication of our study is that it does not seem possible to fit all pallasites within a single genetic frame. While many pallasites clearly resulted from the injection of molten metal into a brecciated dunite layer, others may well be olivine cumulates formed at the core-mantle boundary of a partially or totally molten parent body.

Acknowledgments—The post-doctoral work of K. Saiki in Clermont-Ferrand was supported by research fellowships of the French Government and of the Japan Society for the Promotion of Science for Young Scientists. This study benefitted from discussions with Ariel Provost, Hugues Cabane, and Bertrand Devouard, and from the technical assistance of Jean-Claude Berthelay (preparation of starting materials) and Michèle Veschambre (electron probe microanalysis). Dr. C. B. Moore of the Center for Meteorite Studies at Arizona State University (USA) kindly provided the samples of the Brenham and Eagle Station pallasites displayed in Fig. 1. We are indebted to Susumu Ikeda for his help in communication between France and Japan. We are grateful to Drs. Joseph I. Goldstein, Jeffrey G. Taylor, and Reid F. Cooper for helpful and constructive reviews and comments. The experimental work was supported by the Institut National des Sciences de l'Univers through two grants from programs PNP-97 and PNP-2000. This is INSU-CNRS contribution 340.

Editorial Handling—Dr. Joseph Goldstein

REFERENCES

- Béjina F., Jaoul O., and Liebermann R. C. 1999. Activation volume of Si diffusion in San Carlos olivine: Implications for upper mantle rheology. *Journal of Geophysical Research* 104:25529–25542.
- Boesenberg J. S., Prinz M., Weisberg M. K., Davis A. M., Clayton R. N., Mayeda T. K., and Wasson J. T. 1995. Pyroxene pallasites: A new pallasite grouplet (abstract). *Meteoritics* 30:488–489.
- Burret R. and Sato M. 1984. Intrinsic oxygen fugacity measurements on seven chondrites, a pallasite, and a tektite and the redox state of meteorite parent bodies. *Geochimica et Cosmochimica Acta* 48:111–120.
- Buseck P. R. 1977. Pallasite meteorites—Mineralogy, petrology, and geochemistry. *Geochimica et Cosmochimica Acta* 41:711–740.
- Buseck P. R. and Goldstein J. I. 1969. Olivine compositions and cooling rates of pallasitic meteorites. *Bulletin of the Geological Society of America* 80:2141–2158.
- Cabane H., Laporte D., and Provost A. 2001. Experimental investigation of the kinetics of Ostwald ripening of quartz in silicic melts. *Contributions to Mineralogy and Petrology* 142:361–373.
- Coble R. L. 1963. A model for boundary diffusion controlled creep in polycrystalline materials. *Journal of Applied Physics* 34:1679–1682.
- Greenberg R. and Chapman C. R. 1984. Asteroids and meteorites: Origin of stony-iron meteorites at mantle-core boundaries. *Icarus* 57:267–279.
- Herring C. 1950. Diffusional viscosity of a polycrystalline solid. *Journal of Applied Physics* 21:437–445.
- Jaoul O. 1990. Multicomponent diffusion and creep in olivine. *Journal of Geophysical Research* 95:17631–17642.
- Kern R. 1987. The equilibrium form of a crystal. In *Morphology of crystals*, edited by Sunagawa I. Tokyo: Terra Scientific Publishing Company, pp. 77–206.
- Klosterman M. J. and Buseck P. R. 1973. Structural analysis of olivine in pallasitic meteorites: Deformation in planetary interiors. *Journal of Geophysical Research* 78:7581–7588.
- Laporte D. 1994. Wetting behavior of partial melts during crustal anatexis: The distribution of hydrous silicic melts in polycrystalline aggregates of quartz. *Contributions to Mineralogy and Petrology* 116:486–499.
- Lugmair G. W. and Shukolyukov A. 1998. Early solar system timescales according to ^{53}Mn - ^{53}Cr systematics. *Geochimica et Cosmochimica Acta* 62:2863–2886.
- Miyamoto M. 1997. Chemical zoning of olivine in several pallasites. *Journal of Geophysical Research* 102:21613–21618.
- Miyamoto M. and Takeda H. 1993. Rapid cooling of pallasite: Comparison of chemical zoning with primitive achondrites (abstract). *Meteoritics* 28:404–405.
- Miyamoto M. and Takeda H. 1996. Chemical zoning of olivine in several pallasites suggestive of faster cooling (abstract). 25th Lunar and Planetary Science Conference, pp. 921–922.
- Narayan C. and Goldstein J. I. 1985. A major revision of iron meteorites cooling rates—An experimental study of the growth of Widmanstätten pattern. *Geochimica et Cosmochimica Acta* 49:397–410.
- Ohtani E. 1983. Formation of olivine textures in pallasites and thermal history of pallasites in their parent body. *Physics of the Earth and Planetary Interiors* 32:182–192.
- Poirier J. P. 1985. *Creep of crystals*. Cambridge: Cambridge University Press. 260 p.
- Saiki K. 1997. Morphology and simulation of solid state rounding process. *Geophysical Research Letters* 24:1519–1522.
- Scott E. R. D. 1977a. Pallasites—Metal composition, classification, and relationships with iron meteorites. *Geochimica et Cosmochimica Acta* 41:693–710.
- Scott E. R. D. 1977b. Formation of olivine-metal textures in pallasite meteorites. *Geochimica et Cosmochimica Acta* 41:693–710.
- Shen J. J., Papanastassiou D. A., and Wasserburg G. J. 1998. Re-Os systematics in pallasite and mesosiderite metal. *Geochimica et Cosmochimica Acta* 62:2715–2723.
- Shewmon P. 1963. *Diffusion in solids*. New York: McGraw-Hill. 177 p.
- Smith C. S. 1964. Some elementary principles of polycrystalline microstructure. *Metallurgical Reviews* 9:1–48.
- Sutton A. P. and Balluffi R. W. 1995. *Interfaces in crystalline*

- materials. Oxford: Oxford University Press. 819 p.
- Takahashi E. 1983. Melting of a Yamato L3 chondrite (Y-74191) up to 30 kbar. *Proceedings of the 8th Symposium on Antarctic Meteorites*. pp. 168–180.
- Toriumi M. 1979. A mechanism of shape-transformation of quartz inclusions in albite of regional metamorphic rocks. *Lithos* 12: 325–333.
- Toriumi M. 1981. Rounded mineral inclusions in the upper mantle peridotite. *Physics of the Earth and Planetary Interiors* 27:39–46.
- Ulf-Møller F., Choi B. G., Rubin A. E., Tran J., and Wasson J. T. 1998. Paucity of sulfide in a large slab of Esquel: New perspectives on pallasite formation. *Meteoritics & Planetary Science* 33:221–227.
- Urakawa S., Kato M., and Kumazawa M. 1987. Experimental study on the phase relations in the system Fe-Ni-O-S. *Physics of the Earth and Planetary Interiors* 32:193–202.
- Wasson J. T., Lange D. E., Francis C. A., and Ulf-Møller F. 1999. Massive chromite in the Brenham pallasite and the fractionation of Cr during the crystallization of asteroidal cores. *Geochimica et Cosmochimica Acta* 63:1219–1232.
- Wood J. A. 1978. Nature and evolution of the meteorite parent bodies: Evidence from petrology and metallurgy. In *Asteroids: An exploration assessment*, edited by Morisson D. and Wells W. C. NASA Conference Publication 2053. pp. 45–57.
- Yang C. W., Williams D. B., and Goldstein J. I. 1997. A new empirical cooling rate indicator for meteorites based on the size of the cloudy zone of the metallic phases. *Meteoritics & Planetary Science* 32:423–429.

APPENDIX

The following source is written using Image Macro Language. When using this macro, verify that the pixel value of 0 is assigned as white and the pixel value of 255 is assigned as black. If they are switched, invert the image after binarization.

```

macro 'Area';
var
area:integer;
begin
Measure;
area:=Histogram[255];
PutMessage('area =',area);
end;

macro 'Binarize (area fix)';
var
initarea,area,sumarea:integer;
n:integer;
cycle:integer;
begin
sumarea:=0;
initarea:=GetNumber('Enter target area:',0);
n:=256;
Measure;
while sumarea<initarea do begin
n:=n-1;
sumarea:=sumarea+Histogram[n];
end;

PutMessage('sumarea =',sumarea);
PutMessage('n=',n);

SetThreshold(n);
MakeBinary;
end;

macro '0.5 Gauss';
begin
NewTextWindow('0.5 gauss',160,140);
writeln('0 0 0 0 0 0 0 0 0 0 0 0 0 0 0');
writeln('0 0 0 0 0 0 0 0 0 0 0 0 0 0 0');
writeln('0 0 0 0 0 0 0 0 0 0 0 0 0 0 0');
writeln('0 0 0 0 0 0 0 0 0 0 0 0 0 0 0');
writeln('0 0 0 0 0 0 0 0 0 0 0 0 0 0 0');
Convolve("");
Dispose;
end;

macro '1.0 Gauss';
begin
NewTextWindow('1.0 gauss',160,140);
writeln('0 0 0 0 0 0 0 0 0 0 0 0 0 0 0');
writeln('0 0 0 0 0 0 0 0 0 0 0 0 0 0 0');
writeln('0 0 0 0 0 0 0 0 0 0 0 0 0 0 0');
writeln('0 0 0 0 0 0 0 0 0 0 0 0 0 0 0');
writeln('0 0 0 0 0 0 2 3 2 0 0 0 0 0 0');
writeln('0 0 0 0 2 2 1 9 4 1 5 5 9 4 2 1 2 0 0 0 0');
writeln('0 0 0 0 3 3 5 1 5 5 2 5 5 1 5 5 3 3 0 0 0 0');
writeln('0 0 0 0 2 2 1 9 4 1 5 5 9 4 2 1 2 0 0 0 0');
writeln('0 0 0 0 0 5 2 1 3 5 2 1 5 0 0 0 0 0');
writeln('0 0 0 0 0 2 2 3 2 0 0 0 0 0 0');
writeln('0 0 0 0 0 0 0 0 0 0 0 0 0 0 0');
writeln('0 0 0 0 0 0 0 0 0 0 0 0 0 0 0');
Convolve("");
Dispose;
end;

macro '1.5 Gauss';
begin
NewTextWindow('1.5 gauss',160,140);

```

```

writeln('0 0 0 0 0 0 0 0 0 0 0 0 0 0 0');
writeln('0 0 0 0 0 0 0 0 0 0 0 0 0 0 0');
writeln('0 0 0 0 0 1 1 1 0 0 0 0 0 0');
writeln('0 0 0 0 1 3 6 7 6 3 1 0 0 0 0');
writeln('0 0 0 1 5 14 28 35 28 14 5 1 0 0 0');
writeln('0 0 0 3 14 43 84 105 84 43 14 3 0 0 0');
writeln('0 0 1 6 28 84 164 204 164 84 28 6 1 0 0');
writeln('0 0 1 7 35 105 204 255 204 105 35 7 1 0 0');
writeln('0 0 1 6 28 84 164 204 164 84 28 6 1 0 0');
writeln('0 0 0 3 14 43 84 105 84 43 14 3 0 0 0');
writeln('0 0 0 1 5 14 28 35 28 14 5 1 0 0 0');
writeln('0 0 0 1 3 6 7 6 3 1 0 0 0 0');
writeln('0 0 0 0 0 1 1 1 0 0 0 0 0 0');
writeln('0 0 0 0 0 0 0 0 0 0 0 0 0 0 0');
writeln('0 0 0 0 0 0 0 0 0 0 0 0 0 0 0');
Convolve("");
Dispose;
end;

macro '2.0 Gauss';
begin
NewTextWindow('2.0 gauss',160,140);
writeln('0 0 0 0 0 0 1 0 0 0 0 0 0 0');
writeln('0 0 0 0 1 2 2 3 2 2 1 0 0 0 0');
writeln('0 0 0 2 4 7 10 11 10 7 4 2 0 0 0');
writeln('0 0 2 5 11 21 30 35 30 21 11 5 2 0 0');
writeln('0 1 4 11 27 50 73 83 73 50 27 11 4 1 0');
writeln('0 2 7 21 50 94 136 155 136 94 50 21 7 2 0');
writeln('0 2 10 30 73 136 199 225 199 136 73 30 10 2 0');
writeln('1 3 11 35 83 155 225 255 225 155 83 35 11 3 1');
writeln('0 2 10 30 73 136 199 225 199 136 73 30 10 2 0');
writeln('0 2 7 21 50 94 136 155 136 94 50 21 7 2 0');
writeln('0 1 4 11 27 50 73 83 73 50 27 11 4 1 0');
writeln('0 0 2 5 11 21 30 35 30 21 11 5 2 0 0');
writeln('0 0 0 2 4 7 10 11 10 7 4 2 0 0 0');
writeln('0 0 0 0 1 2 2 3 2 2 1 0 0 0 0');
writeln('0 0 0 0 0 0 1 0 0 0 0 0 0 0');
Convolve("");
Dispose;
end;

macro '2.5 Gauss';
begin
NewTextWindow('2.5 gauss',160,140);
writeln('0 0 1 1 2 4 5 5 5 4 2 1 1 0 0');
writeln('0 1 2 4 7 10 13 14 13 10 7 4 2 1 0');
writeln('1 2 5 10 17 25 32 35 32 25 17 10 5 2 1');
writeln('1 4 10 20 35 51 65 71 65 51 35 20 10 4 1');
writeln('2 7 17 35 60 90 115 124 115 90 60 35 17 7 2');
writeln('4 10 25 51 90 134 171 185 171 134 90 51 25 10 4');
writeln('5 13 32 65 115 171 217 235 217 171 115 65 32 13 5');
writeln('5 14 35 71 124 185 235 255 235 185 124 71 35 14 5');
writeln('5 13 32 65 115 171 217 235 217 171 115 65 32 13 5');
writeln('4 10 25 51 90 134 171 185 171 134 90 51 25 10 4');
writeln('2 7 17 35 60 90 115 124 115 90 60 35 17 7 2');
writeln('1 4 10 20 35 51 65 71 65 51 35 20 10 4 1');
writeln('1 2 5 10 17 25 32 35 32 25 17 10 5 2 1');
writeln('0 1 2 4 7 10 13 14 13 10 7 4 2 1 0');
writeln('0 0 1 1 2 4 5 5 5 4 2 1 1 0 0');
Convolve("");
Dispose;
end;

macro '3.0 Gauss';
begin
NewTextWindow('3.0 gauss',160,140);
writeln('1 2 4 7 10 13 16 17 16 13 10 7 4 2 1');
writeln('2 5 9 14 21 28 33 35 33 28 21 14 9 5 2');
writeln('4 9 16 26 39 51 60 64 60 51 39 26 16 9 4');
writeln('7 14 26 43 64 84 99 105 99 84 64 43 26 14 7');
writeln('10 21 39 64 94 124 146 155 146 124 94 64 39 21 10');
writeln('13 28 51 84 124 164 193 204 193 164 124 84 51 28 13');
writeln('16 33 60 99 146 193 228 241 228 193 146 99 60 33 16');
writeln('17 35 64 105 155 204 241 255 241 204 155 105 64 35 17');
writeln('16 33 60 99 146 193 228 241 228 193 146 99 60 33 16');
writeln('13 28 51 84 124 164 193 204 193 164 124 84 51 28 13');
writeln('10 21 39 64 94 124 146 155 146 124 94 64 39 21 10');
writeln('7 14 26 43 64 84 99 105 99 84 64 43 26 14 7');
writeln('4 9 16 26 39 51 60 64 60 51 39 26 16 9 4');
writeln('2 5 9 14 21 28 33 35 33 28 21 14 9 5 2');
writeln('1 2 4 7 10 13 16 17 16 13 10 7 4 2 1');
Convolve("");
Dispose;
end;

macro '3.5 Gauss';
begin
NewTextWindow('3.5 gauss',160,140);
writeln('5 8 12 18 24 29 33 35 33 29 24 18 12 8 5');
writeln('8 13 21 31 41 50 56 59 56 50 41 31 21 13 8');
writeln('12 21 33 48 64 78 88 92 88 78 64 48 33 21 12');
writeln('18 31 48 69 92 113 127 133 127 113 92 69 48 31 18');
writeln('24 41 64 92 122 150 170 177 170 150 122 92 64 41 24');
writeln('29 50 78 113 150 184 208 217 208 184 150 113 78 50 29');
writeln('33 56 88 127 170 208 235 245 235 208 170 127 88 56 33');
writeln('35 59 92 133 177 217 245 255 245 217 177 133 92 59 35');
writeln('33 56 88 127 170 208 235 245 235 208 170 127 88 56 33');
writeln('29 50 78 113 150 184 208 217 208 184 150 113 78 50 29');
writeln('24 41 64 92 122 150 170 177 170 150 122 92 64 41 24');
writeln('18 31 48 69 92 113 127 133 127 113 92 69 48 31 18');
writeln('12 21 33 48 64 78 88 92 88 78 64 48 33 21 12');
writeln('8 13 21 31 41 50 56 59 56 50 41 31 21 13 8');
writeln('5 8 12 18 24 29 33 35 33 29 24 18 12 8 5');
Convolve("");
Dispose;
end;

macro '4.0 Gauss';
begin
NewTextWindow('4.0 gauss',160,140);
writeln('12 18 25 33 42 49 53 55 53 49 42 33 25 18 12');
writeln('18 27 38 50 62 73 80 83 80 73 62 50 38 27 18');
writeln('25 38 53 71 88 103 113 117 113 103 88 71 53 38 25');
writeln('33 50 71 94 117 136 150 155 150 136 117 94 71 50 33');
writeln('42 62 88 117 145 170 187 192 187 170 145 117 88 62 42');
writeln('49 73 103 136 170 199 218 225 218 199 170 136 103 73 49');
writeln('53 80 113 150 187 218 240 247 240 218 187 150 113 80 53');
writeln('55 83 117 155 192 225 247 255 247 225 192 155 117 83 55');

```

```
writeln('53 80 113 150 187 218 240 247 240 218 187 150 113 80 53');  
writeln('49 73 103 136 170 199 218 225 218 199 170 136 103 73 49');  
writeln('42 62 88 117 145 170 187 192 187 170 145 117 88 62 42');  
writeln('33 50 71 94 117 136 150 155 150 136 117 94 71 50 33');  
writeln('25 38 53 71 88 103 113 117 113 103 88 71 53 38 25');  
writeln('18 27 38 50 62 73 80 83 80 73 62 50 38 27 18');  
writeln('12 18 25 33 42 49 53 55 53 49 42 33 25 18 12');  
Convolve("");  
Dispose;  
end;
```

```
macro '4.5 Gauss';  
begin  
NewTextWindow('4.5 gauss',160,140);  
writeln('23 31 41 51 61 69 74 76 74 69 61 51 41 31 23');  
writeln('31 43 57 71 84 95 102 105 102 95 84 71 57 43 31');
```

```
writeln('41 57 74 93 110 125 134 138 134 125 110 93 74 57 41');  
writeln('51 71 93 116 138 156 168 172 168 156 138 116 93 71 51');  
writeln('61 84 110 138 164 185 199 204 199 185 164 138 110 84 61');  
writeln('69 95 125 156 185 209 225 231 225 209 185 156 125 95 69');  
writeln('74 102 134 168 199 225 243 249 243 225 199 168 134 102 74');  
writeln('76 105 138 172 204 231 249 255 249 231 204 172 138 105 76');  
writeln('74 102 134 168 199 225 243 249 243 225 199 168 134 102 74');  
writeln('69 95 125 156 185 209 225 231 225 209 185 156 125 95 69');  
writeln('61 84 110 138 164 185 199 204 199 185 164 138 110 84 61');  
writeln('51 71 93 116 138 156 168 172 168 156 138 116 93 71 51');  
writeln('41 57 74 93 110 125 134 138 134 125 110 93 74 57 41');  
writeln('31 43 57 71 84 95 102 105 102 95 84 71 57 43 31');  
writeln('23 31 41 51 61 69 74 76 74 69 61 51 41 31 23');  
Convolve("");  
Dispose;  
end;
```
